Eur. Phys. J. A (2016) **52**: 48
DOI 10.1140/epja/i2016-16048-7

THE EUROPEAN PHYSICAL JOURNAL A

Regular Article – Theoretical Physics

Electric dipole excitation of ^{208}Pb by polarized electron impact

D.H. Jakubassa-Amundsen[1] and V.Yu. Ponomarev[2,a]

[1] Mathematics Institute, University of Munich, Theresienstrasse 39, 80333 Munich, Germany
[2] Institut für Kernphysik, Technische Universität Darmstadt, D-64289 Darmstadt, Germany

Received: 3 December 2015 / Revised: 15 January 2016
Published online: 14 March 2016 – © Società Italiana di Fisica / Springer-Verlag 2016
Communicated by H. Wittig

Abstract. The cross sections and spin asymmetries for the excitation of 1^- states in ^{208}Pb by transversely polarized electrons with collision energy of 30–180 MeV have been examined within the DWBA scattering formalism. As examples, we have considered a low-lying 1^- state and also states belonging to the pygmy dipole and giant dipole resonances. The structure of these states and their corresponding transition charge and current densities have been taken from an RPA calculation within the quasiparticle phonon model. The complex-plane rotation method has been applied to achieve the convergence of the radial DWBA integrals for backward scattering. We have studied the behaviour of the cross sections and spin asymmetries as a function of electron energy and scattering angle. The role of the longitudinal and transversal contributions to the excitation has been thoroughly studied. We conclude that the spin asymmetry S, related to unpolarized outgoing electrons, is mostly well below 1% even at the backward scattering angles and its measurement provides a challenge for future experiments with polarized electrons.

1 Introduction

Inelastic scattering of electrons is a powerful tool in nuclear physics. The well-known mechanism of their interaction with target nuclei allows to extract nuclear structure information in a model-independent way. The possibility to vary the momentum transfer in this reaction by changing the energy of the beam electrons and/or the scattering angle of the detected electrons allows to select the conditions under which the states of different multipolarities are preferably excited.

The investigation of low-lying 1^- excited states in nuclei, which are often referred to as the pygmy dipole resonance (PDR), is one of the hot topics in nuclear structure studies of the last decade. The PDR was first observed in experiments with tagged photons (see, *e.g.* [1, 2]) as a substructure on the low-energy tail of the giant dipole resonance (GDR). In the late 1990s the fine structure of the PDR, being composed of a hundred of 1^- states, has been resolved in nuclear resonance fluorescence (NRF) measurements [3, 4]. From those days the PDR has been intensively studied in different parts of the nuclear chart not only in the NRF experiments with unpolarized and polarized photons but also in other nuclear reactions like $(\alpha, \alpha'\gamma)$ [5, 6] or heavy ion collisions [7, 8] as well. For a detailed review of these studies we refer to [9].

Inelastic scattering of electrons with an energy of 50–100 MeV may also provide its contribution to the PDR studies. Some data on the observation of 1^- states in (e, e') reactions is available (see, *e.g.* [10, 11]) but in general, this information is very sparse. The required electron energy can be provided by the S-DALINAC in Darmstadt (Germany) where the detector system allows for measurements in a wide range of scattering angles, including the backward scattered electrons close to 180° which can be detected with high angular resolution [12]. Moreover, a new set-up has recently been installed at the S-DALINAC which allows to perform experiments with polarized electrons [13].

The goal of this paper is to provide an estimate of the results which one may expect from inelastic scattering of polarized electrons leading to the excitation of low-lying 1^- states. As an example we have selected the well-known 1^- state in ^{208}Pb with an energy of 5.512 MeV, and a 1^- state at a slightly higher energy (7.5 MeV) which belongs to the PDR. For comparison, we have also considered a 1^- state from the GDR region. The cross section of the reaction is calculated within the standard distorted-wave Born approximation (DWBA) [14], which accounts for the Coulomb distortion of the electronic scattering states. The respective nuclear transition charge and current densities are calculated within the quasiparticle phonon model (QPM) which describes rather well the 1^- states in ^{208}Pb [15, 16].

Another motivation of our theoretical work concerns the predictions for the spin asymmetry which is known from elastic scattering to be particularly large for heavy

[a] e-mail: ponomare@crunch.ikp.physik.tu-darmstadt.de

nuclei and backmost scattering angles. In fact, there exist no systematic measurements on the spin asymmetry in the low-energy region (apart from its angular distribution at 14 MeV for elastic ^{208}Pb(e,e') scattering [17]). Any comparison between experiment and proper calculations is therefore missing, in particular for inelastic electron scattering. Such tests of theoretical models with the kinematics of the S-DALINAC may also help to understand discrepancies between theory and experiment at ultrahigh energies [18]. Since at scattering angles near 180° the momentum transfer is quite large even at moderate collision energies, the importance of the two-photon exchange (in the sense of excited intermediate nuclear states) or of other perturbative effects is unclear. Therefore a reproduction of our theoretical predictions by experiment is by no means trivial. One should also keep in mind that the information on the nuclear properties extracted from the spin asymmetry is complementary to the information extracted from the form factors due to its additional sensitivity to the structure of the nuclear wave functions or to interference effects [19–21]. Hence the spin asymmetry allows for a more stringent test of the nuclear models than mere cross section measurements.

In approaching the scattering angle of 180° we face an old problem that the radial integrals hardly converge for multipolarities 0 (which occur in the contribution from the transition current density J_{10}). We suggest a solution of this problem by using the complex-plane rotation method (CRM) instead of performing the integration along the real axis. This method was introduced in its non-relativistic version in the context of (d,p) reactions [22] and was generalized for bremsstrahlung emission in relativistic electron-atom collisions to the case of fast electrons scattering from heavy point nuclei [23]. In the present work we provide an extension of the CRM to account for scattering from extended nuclei.

The paper is organized as follows. Section 2 gives a short account of the DWBA scattering formalism and introduces the CRM. The nuclear model for the transition densities is described in sect. 3. Results for the selected 1^- excitations of ^{208}Pb are presented in sect. 4. The conclusion is drawn in sect. 5. Atomic units ($\hbar = m = e = 1$) are used unless indicated otherwise. In particular, the electron mass m is retained throughout.

2 DWBA formalism and the complex-plane rotation method

Let us describe the excitation of a nucleus with initial angular momentum quantum numbers J_i, M_i to a final state characterized by J_f, M_f. Let us consider transitions with only one multipolarity L. The differential cross section for the excitation by electrons with initial spin polarization $\boldsymbol{\zeta}_i$ and final spin polarization $\boldsymbol{\zeta}_f$ is obtained from [14, 24]

$$\frac{\mathrm{d}\sigma}{\mathrm{d}\Omega}(\boldsymbol{\zeta}_i,\boldsymbol{\zeta}_f) = \frac{k_f}{k_i}\,\frac{1}{f_{\mathrm{rec}}}\,\frac{4\pi^3 E_i E_f}{c^2} \times \frac{1}{2J_i+1}\sum_{M_i,M_f}\left|A_{fi}^{\mathrm{coul}}(M_i,M_f)+A_{fi}^{\mathrm{mag}}(M_i,M_f)\right|^2, \quad (1)$$

where f_{rec} is the recoil term arising from the finite mass of the target nucleus. Assuming that the polarization of the nucleus is not observed, an average over M_i and a sum over M_f is included. The transition amplitudes for Coulomb and magnetic scattering are given by [14, 25, 26]

$$\begin{aligned} A_{fi}^{\mathrm{coul}}(M_i,M_f) &= -\frac{1}{c}\int \mathrm{d}\boldsymbol{r}_N \mathrm{d}\boldsymbol{r}_e \left(\psi_f^{(\sigma_f)\dagger}(\boldsymbol{r}_e)\,\psi_i^{(\sigma_i)}(\boldsymbol{r}_e)\right) \\ &\quad\times \frac{e^{ik|\boldsymbol{r}_e-\boldsymbol{r}_N|}}{|\boldsymbol{r}_e-\boldsymbol{r}_N|}\sqrt{4\pi}\,\varrho_{fi}(\boldsymbol{r}_N) \\ A_{fi}^{\mathrm{mag}}(M_i,M_f) &= \frac{1}{c}\int \mathrm{d}\boldsymbol{r}_N \mathrm{d}\boldsymbol{r}_e \left(\psi_f^{(\sigma_f)\dagger}(\boldsymbol{r}_e)\,\boldsymbol{\alpha}\,\psi_i^{(\sigma_i)}(\boldsymbol{r}_e)\right) \\ &\quad\times \frac{\overleftrightarrow{I}\; e^{ik|\boldsymbol{r}_e-\boldsymbol{r}_N|}}{|\boldsymbol{r}_e-\boldsymbol{r}_N|}\sqrt{4\pi}\,\boldsymbol{j}_{fi}(\boldsymbol{r}_N), \end{aligned} \quad (2)$$

where $\boldsymbol{r}_e$ and $\boldsymbol{r}_N$ are electron and nuclear coordinate, respectively, $k = E_x/c$, with E_x the nuclear excitation energy, $\boldsymbol{k}_i$, σ_i, E_i and $\boldsymbol{k}_f$, σ_f, E_f are the initial and final momentum, spin projection and total energy of the electron, respectively, $\boldsymbol{\alpha}$ is the vector of Dirac matrices and $\overleftrightarrow{I}$ the dyadic unit matrix.

For the nuclear transition matrix elements ϱ_{fi} and $\boldsymbol{j}_{fi}$ multipole expansions are conventionally made [27, 28]. Introducing the transition charge density ϱ_L and the transition current densities $J_{L,L\pm1}$ (*i.e.* restricting ourselves to transverse electric excitations as described in sect. 3), these are given by

$$\begin{aligned} \varrho_{fi}(\boldsymbol{r}_N) &= \sum_{M=-L}^{L}(J_iM_i\,LM|J_fM_f)\,\varrho_L(r_N)\,Y_{LM}^*(\hat{\boldsymbol{r}}_N), \\ \boldsymbol{j}_{fi}(\boldsymbol{r}_N) &= -i\sum_{\lambda=L\pm1}\sum_{M=-L}^{L}(J_iM_i\,LM|J_fM_f) \\ &\quad\times J_{L\lambda}(r_N)\,\boldsymbol{Y}_{L\lambda}^{M*}(\hat{\boldsymbol{r}}_N), \end{aligned} \quad (3)$$

where Y_{LM} and $\boldsymbol{Y}_{L\lambda}^M$ are spherical harmonics and vector spherical harmonics, respectively, multiplied by Clebsch-Gordan coefficients [29]. These assure that for spin-zero nuclei ($J_i = 0$) such as ^{208}Pb, one has $L = J_f$ and $M = M_f$.

For the propagator as well as for the electronic scattering states $\psi_i^{(\sigma_i)}$ and $\psi_f^{(\sigma_f)}$ a partial-wave expansion is made [14, 27]. The radial functions are obtained by solving the Dirac equation for the electron in the nuclear potential (derived from a Fourier-Bessel expansion of the ^{208}Pb ground-state charge density [30]) with the help of the Fortran code RADIAL of Salvat *et al.* [31]. In this code the radial step size should be reduced for the higher collision energies.

The infinite electronic radial integrals occurring in the DWBA formalism are of the type [14, 32]

$$\int_{R_m}^{\infty}\mathrm{d}r_e r_e^2\,h_\lambda^{(1)}(kr_e)\,D(r_e), \quad (4)$$

where R_m is some distance outside the nuclear transition density distributions, $h_\lambda^{(1)}$ (with $\lambda \geq 0$) is a spherical Hankel function of the first kind and $D(r_e)$ denotes a product

of radial Dirac functions. Along the real axis the integrand in (4) is strongly oscillating with a weak asymptotic decrease ($\sim 1/r_e$). The numerical convergence problems, which are particularly large for $\lambda = 0$ [32], can be circumvented by deforming the contour into the complex plane as described in [22]. To do so, we recall that $D(r)$ consists of functions which are linear combinations of regular and irregular Coulomb-Dirac functions [31, 33], provided R_m is large enough such that it is outside the grid defined by RADIAL (*i.e.* well outside the range of the short-range part of the potential),

$$\begin{pmatrix} g_\kappa \\ f_\kappa \end{pmatrix} = \cos\delta_\kappa \begin{pmatrix} g_\kappa \\ f_\kappa \end{pmatrix}^{\rm reg} + \sin\delta_\kappa \begin{pmatrix} g_\kappa \\ f_\kappa \end{pmatrix}^{\rm irr}, \qquad (5)$$

where δ_κ is the phase shift caused by the short-range part of the potential, g_κ is the large and f_κ is the small component of the radial Dirac function. As shown in the appendix, these functions can for sufficiently large distances readily be continued into the complex plane, where they can be split into a sum of two terms, one behaving asymptotically like e^{ikz}, the other like e^{-ikz} (with k equal to k_i or k_f), according to

$$\begin{aligned} g_\kappa(z) &\equiv g_\kappa^{(+)}(e^{ikz}) + g_\kappa^{(-)}(e^{-ikz}) \\ f_\kappa(z) &\equiv f_\kappa^{(+)}(e^{ikz}) + f_\kappa^{(-)}(e^{-ikz}). \end{aligned} \qquad (6)$$

If $D(r)$ consists just of regular Coulomb-Dirac functions (*i.e.* in the case of point nuclei or for large relativistic quantum numbers κ_i and κ_f) the above splitting was derived in [23]. The Hankel function in (4) behaves like $h_\lambda^{(1)}(kz) \sim e^{ikz}$ (with a bounded coefficient for $|z| \geq R_m$). Therefore the deformed contour, starting at R_m and following the positive, respectively negative imaginary axis to infinity, can be closed along the infinitely far semicircle in the upper and lower half plane, respectively. According to [22, 23], a necessary condition for this method to work is that

$$\Delta k = k_i - k_f - k > 0, \qquad (7)$$

which holds for nuclear excitation (provided the electron mass m is retained). It follows that this method does not work for elastic ($k = 0$), recoil-free ($k_f = k_i$) electron scattering. From (7) it follows that the sign of the exponential $e^{\pm ik_i z}$ determines exponential growth or decay for imaginary z. Therefore it is sufficient to use the decomposition (6) only for the initial scattering state. Substituting $r \equiv z = R_m + iy$ in the integral involving $g_{\kappa_i}^{(+)}$ and $r = R_m - iy$ in the integral involving $g_{\kappa_i}^{(-)}$, one obtains, for example,

$$\begin{aligned} &\int_{R_m}^{\infty} {\rm d}r\, r^2\, g_{\kappa_i}(r) f_{\kappa_f}(r)\, h_\lambda^{(1)}(kr) = \\ &i\int_0^{\infty} {\rm d}y\, r^2\, g_{\kappa_i}^{(+)}(e^{ik_i r}) f_{\kappa_f}(r)\, h_\lambda^{(1)}(kr)\Big|_{r=R_m+iy} \\ &-i\int_0^{\infty} {\rm d}y\, r^2\, g_{\kappa_i}^{(-)}(e^{-ik_i r}) f_{\kappa_f}(r)\, h_\lambda^{(1)}(kr)\Big|_{r=R_m-iy}, \end{aligned} \qquad (8)$$

with $f_{\kappa_f}(r)$ from (A.7). The upper integration limit, necessary for convergence, is determined by $y_{\max} \sim 8/\Delta k$ with Δk from (7), which is even larger than suggested in [34].

For very small Δk, leading to very large $y_{\max}$, (8) actually has to be modified. Let us take for example the collision energy $E_{i,\rm kin} = E_i - c^2 = 70\,{\rm MeV}$, $\theta = 175°$ and $E_x = 5.5\,{\rm MeV}$. Then one has $k_i = 1.9 \times 10^4$ a.u. but, including recoil for ^{208}Pb, $\Delta k = 12.6$ a.u., so that $y_{\max} \sim 1$ a.u. Thus the terms in the integrand of (8) which behave like $e^{i(k_i+k_f+k)r}$ or $e^{-i(k_i+k_f-k)r}$ lead to exponential overflow. Therefore, the upper integration limit in (8) should be reduced to $y_{\rm mit} \lesssim 10^{-2}$ a.u., the smaller, the higher E_i, leaving a tail contribution from $y_{\rm mit}$ to $y_{\max}$. In this tail, the final-state wave function should also be split according to (6), retaining only $f_{\kappa_f}^{(-)}$ in the first integral of (8) and $f_{\kappa_f}^{(+)}$ in the second one. Moreover, all appearing functions should be defined without the corresponding exponentials, while $e^{i\Delta kr}$ and $e^{-i\Delta kr}$, respectively, should be introduced as an additional factor in the integrand. With this procedure, excellent convergence of the radial integrals is achieved, even for large $|\kappa|$. This leads also to a fast convergence of the partial-wave series for the cross section. When the Yennie *et al.* convergence acceleration is applied [14, 33], a cutoff at angular momentum $l_{f,\max} \sim 15$–25 is sufficient for the collision energies under consideration.

The difference between the results using the CRM on one hand and real integration paths on the other hand with identical parameters (*i.e.* applying the E_i- and θ-dependent cutoffs $r_e \leq 4/\Delta k$ as well as $l_f \leq l_{f,\max}$, where $l_f = |\kappa_f + \frac{1}{2}| - \frac{1}{2}$, as determined within the CRM) is shown in fig. 1. Notice that the integration along the real paths yields artificial fluctuations in both, differential cross section and spin asymmetry (thin dotted lines in fig. 1), especially at the higher energies of the electrons. The CRM approach is free from these problems (solid lines in fig. 1) and its computation time is up to a factor of 100 shorter.

3 The quasiparticle phonon model

We have used for our studies transition charge and current densities obtained within the quasiparticle phonon model (QPM) [35]. The model Hamiltonian consists of three terms corresponding to a mean field for protons and neutrons, monopole pairing and residual interaction which is taken in a separable Bohr-Mottelson form. Excited states of even-even nuclei are treated as phonons and are obtained from the solution of the quasiparticle RPA equations. The nuclear charge $\varrho_{Li}(r_N)$ and current $J_{L\lambda i}(r_N)$ densities of the i-th one-phonon state with multipolarity L have the form

$$\varrho_{Li}(r_N) = \sum_{jj'}^{n,p} (u_j v_{j'} + v_j u_{j'}) \left(X_{jj'}^{Li} + Y_{jj'}^{Li}\right) \varrho_{jj'}^{L}(r_N) \qquad (9)$$

$$J_{L\lambda i}(r_N) = \sum_{jj'}^{n,p} (u_j v_{j'} - v_j u_{j'}) \left(X_{jj'}^{Li} - Y_{jj'}^{Li}\right) J_{jj'}^{L\lambda}(r_N), \qquad (10)$$

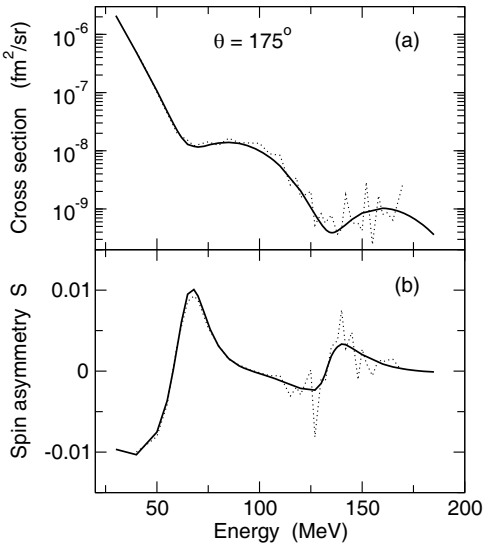

Fig. 1. (a) Differential cross section and (b) spin asymmetry for the excitation of the 1^- state at 5.5 MeV in ^{208}Pb at a scattering angle $\theta = 175°$ as a function of collision energy. Shown are the results from the CRM (solid line) and from performing the radial integrals along the real axis (thin dotted line). The DWBA calculations have been performed neglecting the magnetization current.

where u_j and v_j are the coefficients of the Bogoliubov transformation from particles to quasiparticles (their squares are the occupation numbers for holes and particles, respectively, in non-magic nuclei) and X and Y are the forward and backward amplitudes in the definition of the phonon operator,

$$Q^\dagger_{LMi} = \sum_{jj'}^{n,p} \left(X^{Li}_{jj'} [\alpha^\dagger_j \alpha^\dagger_{j'}]_{LM} - (-1)^{L-M} Y^{Li}_{jj'} [\alpha_{j'} \alpha_j]_{L-M} \right), \tag{11}$$

built up of the quasiparticle ($\alpha^\dagger_{jm}$) pairs,

$$[\alpha^\dagger_j \alpha^\dagger_{j'}]_{LM} = \sum_{mm'} (jmj'm'|LM) \alpha^\dagger_{jm} \alpha^\dagger_{j'm'}. \tag{12}$$

The quantities $\varrho^L_{jj'}(r_N)$ and $J^{L\lambda}_{jj'}(r_N)$ in eqs. (9) and (10) are the particle-hole charge and current transition densities, respectively. The first one has the form,

$$\varrho^L_{jj'}(r_N) = (-)^{j+L-1/2}\, i^{l'-l+L}\, \frac{\hat{j}\hat{j}'(j\tfrac{1}{2}\, j'-\tfrac{1}{2}|L0)}{\sqrt{4\pi}\hat{L}} \times R^*_j(r_N) R_{j'}(r_N); \quad \hat{j} = \sqrt{2j+1}, \tag{13}$$

where $R_j(r_N)$ is the radial part of a single-particle wave function for the mean field level $j \equiv \{nlj\}$. The current particle-hole transition density $J^{L\lambda}_{jj'}(r_N)$ is more complex and we refer for its explicit expression to [27].

The natural parity (or electric) states are described by the charge and current transition densities with $\lambda = L \pm 1$. In the case of unnatural parity (or magnetic) states only the current with $\lambda = L$ is involved. Each nuclear current is composed of a convection part $J^{\rm conv}_{L\lambda i}$ and a magnetization part $J^{\rm mag}_{L\lambda i}$ according to

$$J_{L\lambda i}(r_N) = J^{\rm conv}_{L\lambda i}(r_N) + J^{\rm mag}_{L\lambda i}(r_N). \tag{14}$$

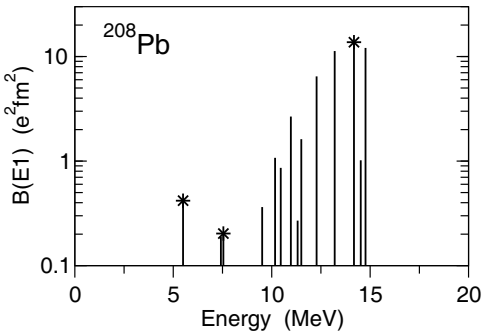

Fig. 2. QPM prediction for the $B(E1\uparrow)$ strength distribution in ^{208}Pb. The three selected states are marked by an asterix.

We have applied the formalism of the previous section to study the excitation of 1^- states in ^{208}Pb in inelastic scattering of polarized electrons. The nuclear structure calculations have been performed with the same set of parameters as in ref. [15]. To exclude the centre of mass motion for the 1^- states we have used effective charges $e_z = N/A$ and $e_n = -Z/A$ for the protons and neutrons, respectively. Effective g-factors, $g^{\rm eff}_s = 0.8 g^{\rm free}_s$, have been used in the calculation of the magnetization current. The Bogoliubov coefficients u_j and v_j are either 0 or 1 for the double-magic nucleus ^{208}Pb.

The $B(E1\uparrow)$ strength distribution from these calculations are displayed in fig. 2. For our future studies we have selected three 1^- states marked with an asterix in this figure. The lowest 1^- state in fig. 2 with energy 5.497 MeV and $B(E1\uparrow) = 0.418\,{\rm e}^2{\rm fm}^2$ corresponds to the experimental level at 5.512 MeV. This is a weakly collective state with dominant contribution of the neutron $\{2f^{-1}_{7/2}\ 2g_{9/2}\}$ and $\{3p^{-1}_{1/2}\ 4s_{1/2}\}$ particle-hole components. The second 1^- state, at 7.5 MeV with $B(E1\uparrow) = 0.203\,{\rm e}^2{\rm fm}^2$, belongs to the PDR. It is a collective state characterized by a destructive interference between many neutron and proton 1p1h-configurations. The third 1^- candidate is a high-lying state at 14.2 MeV with $B(E1\uparrow) = 13.7\,{\rm e}^2{\rm fm}^2$. It represents the GDR states with a typical constructive interference.

The transition charge and current densities for these states are shown in fig. 3. It is seen that the current densities are very large for the two lower states, while the GDR state is dominated by the charge density which is strongly peaked at the nuclear surface. For the state at 7.5 MeV, the charge density has only a tail contribution at the nuclear surface such that it will play a minor role at low collision energies. Correspondingly, the (e, e') results for these three states are very different (see the next section).

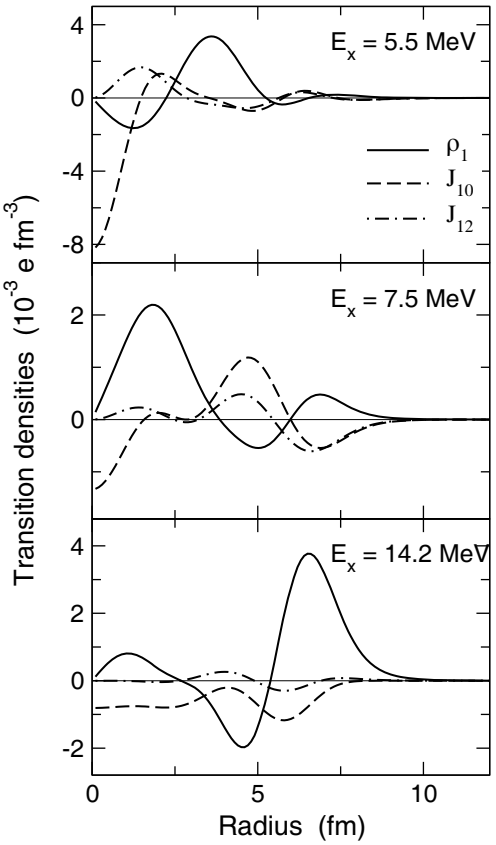

Fig. 3. Transition charge density ϱ_1 (solid line) and transition current densities J_{10} (dashed line) and J_{12} (dash-dotted line) as a function of the nuclear coordinate r_N for the excitation of the 1^- states in ^{208}Pb at $E_x = 5.5\,\mathrm{MeV}$ (upper panel), $E_x = 7.5\,\mathrm{MeV}$ (middle panel) and $E_x = 14.2\,\mathrm{MeV}$ (lower panel). The sign of J_{10} is chosen in accord with [28].

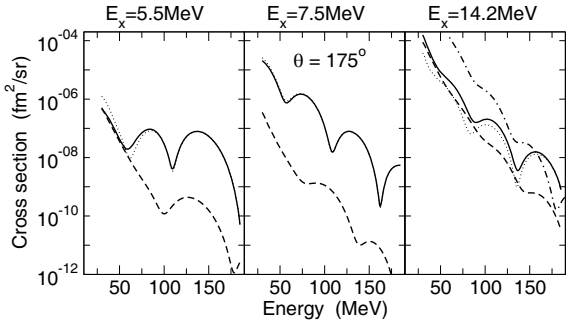

Fig. 4. Differential cross section $(\mathrm{d}\sigma/\mathrm{d}\Omega)_0$ for the excitation of the 1^- states of energy 5.5 MeV (left panel), 7.5 MeV (middle panel) and 14.2 MeV (right panel) in ^{208}Pb at a scattering angle of 175° as a function of kinetic electron energy $E_{i,\mathrm{kin}}$ ($1\,\mathrm{fm}^2/\mathrm{sr} = 10^{-2}\,\mathrm{b/sr}$). Shown is the total cross section (solid lines) as well as the charge contribution (dashed lines) and the transverse electric contribution (thin dotted lines). The result from elastic potential scattering [36] is shown by the dash-dotted line in the right panel.

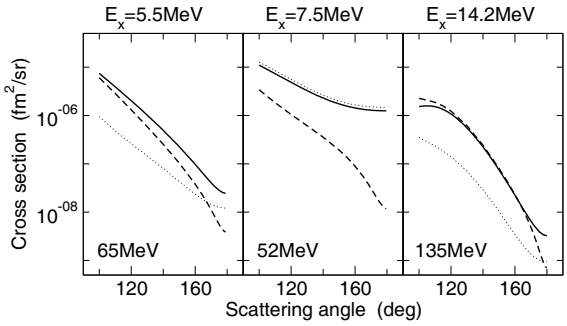

Fig. 5. Differential cross section $(\mathrm{d}\sigma/\mathrm{d}\Omega)_0$ for the excitation of the 1^- states in ^{208}Pb as a function of scattering angle θ. Left panel: $E_x = 5.5\,\mathrm{MeV}$ at impact energy 65 MeV. Middle panel: $E_x = 7.5\,\mathrm{MeV}$ at impact energy 52 MeV. Right panel: $E_x = 14.2\,\mathrm{MeV}$ at impact energy 135 MeV. Shown is the total cross section (solid lines) as well as the charge contribution (dashed lines) and the transverse electric contribution (thin dotted lines).

4 Results

Figure 4 shows the energy dependence of the excitation cross sections for unpolarized electrons, $(\mathrm{d}\sigma/\mathrm{d}\Omega)_0$, at a scattering angle of 175°. At this backward angle the excitation cross sections are only well below the cross section for elastic scattering for energies smaller than 120 MeV, while they may become dominant at the higher collision energies. The oscillations are diffraction structures which evolve at energies sufficiently high such that the electron can penetrate the nuclear surface and scatter from the individual nucleons. The figure also indicates that Coulomb scattering is completely unimportant for the PDR state and loses its importance for the 5.5 MeV state at energies above 60 MeV. The 14.2 MeV excitation, in contrast, is composed of nearly equal contributions from Coulomb and magnetic scattering, at least up to 140 MeV.

The angular dependence of the excitation cross sections for the three states (at collision energies where the spin asymmetry is comparatively large) is displayed in fig. 5. There are two features which are different from the behaviour of higher multipole excitations. In contrast to the plane-wave Born approximation where Coulomb and magnetic scattering add incoherently, the DWBA shows for low multipolarities a significant coherence between these two scattering processes [37]. For the 5.5 MeV state at a collision energy of 65 MeV, for example, it is seen that at large angles the excitation cross section exceeds the sum of Coulomb and magnetic contributions. On the other hand, the total cross section may fall below its magnetic contribution (for the 7.5 MeV state at 52 MeV) or below the Coulomb contribution (for the 14.2 MeV state at 135 MeV below 160°). The second feature concerns the comparatively large value of the Coulomb scattering at the backmost angles, which flattens towards 180° in contrast to the rapid decrease in the plane-wave Born approximation. Similar enhancements of the Coulomb contribution within the DWBA had been found for particular $L = 2$ excitations of ^{181}Ta and ^{166}Er at 180° [37]. This invalidates the common method of extracting nuclear current densities from 180° measurements [38].

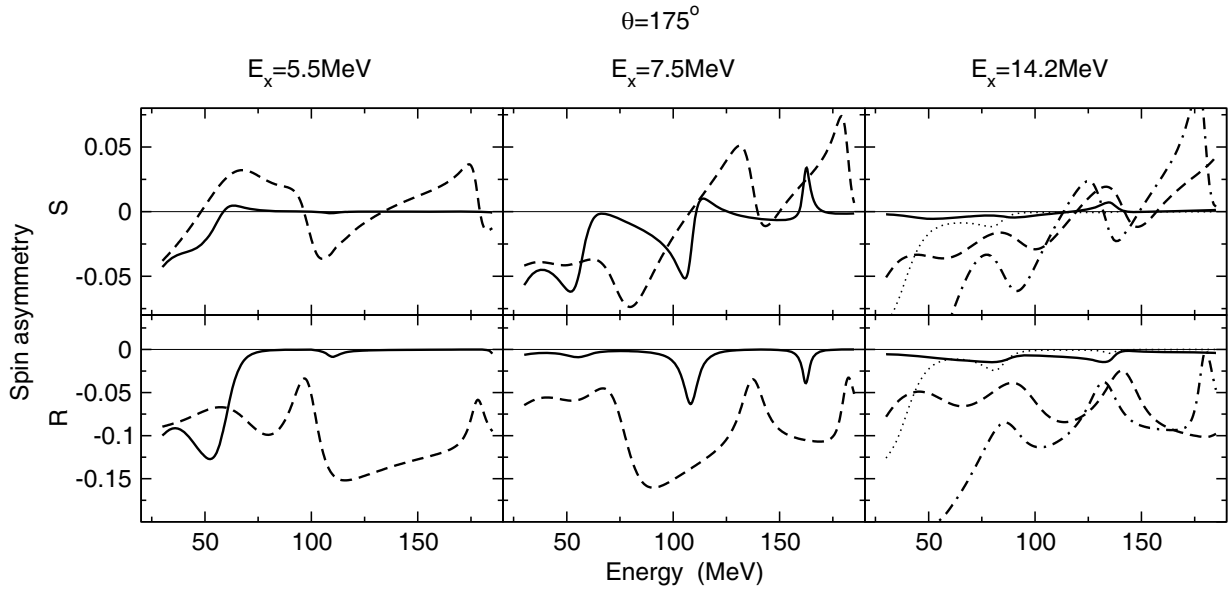

Fig. 6. Top: Sherman function S; bottom: polarization correlation R for the excitation of the 1^- states in ^{208}Pb of energy 5.5 MeV (left panel), 7.5 MeV (middle panel) and 14.2 MeV (right panel) at $\theta = 175°$ as a function of kinetic electron energy $E_{i,\mathrm{kin}}$. The spin asymmetry for the total excitation process is shown by the solid line. Included are the results from the charge contribution (dashed line) and from the transverse electric contribution (thin dotted line). For the 7.5 MeV state, the complete results (solid line) are multiplied by a factor of 100 for S and by 10 for R. Elastic scattering results are presented by the dash-dotted line on the right panel.

In the following we give predictions for the spin asymmetry [39] which is defined by [32]:

$$P(\boldsymbol{\zeta}_i) = \frac{\mathrm{d}\sigma(\boldsymbol{\zeta}_i, \boldsymbol{\zeta}_f) - \mathrm{d}\sigma(-\boldsymbol{\zeta}_i, \boldsymbol{\zeta}_f)}{\mathrm{d}\sigma(\boldsymbol{\zeta}_i, \boldsymbol{\zeta}_f) + \mathrm{d}\sigma(-\boldsymbol{\zeta}_i, \boldsymbol{\zeta}_f)}\,, \tag{15}$$

with $\mathrm{d}\sigma(\boldsymbol{\zeta}_i, \boldsymbol{\zeta}_f)$ abbreviating the differential cross section from (1). If the beam electrons are polarized perpendicular to the scattering plane (*i.e.* $\boldsymbol{\zeta}_i = \hat{\boldsymbol{k}}_i \times \hat{\boldsymbol{k}}_f \equiv \boldsymbol{e}_y$) the rhs of (15) is independent of $\boldsymbol{\zeta}_f$ and defines the so-called Sherman function $S = P(\boldsymbol{e}_y)$ (also called analyzing power). If, on the other hand, $\boldsymbol{\zeta}_i$ lies in the scattering plane perpendicular to the beam axis ($\boldsymbol{\zeta}_i = \hat{\boldsymbol{k}}_i \times \boldsymbol{e}_y \equiv -\boldsymbol{e}_x$) and the final electron is in a helicity (+) state, the rhs of (15) defines the polarization correlation $R = P(-\boldsymbol{e}_x)$.

The energy dependence of S at the scattering angle $\theta = 175°$ is displayed in fig. 6 (top part). As compared to the spin asymmetry in elastic scattering it is considerably reduced, particularly when the magnetic contribution dominates the cross section. The quenching of S due to the magnetic scattering (also present for excitation of higher multipolarities [32]) is made evident by considering the spin asymmetry from the Coulomb scattering alone. This contribution is quite large, in some regions even of similar magnitude as S for elastic scattering.

For the lowest state an appreciable (total) spin asymmetry exists only below 60 MeV at this angle, while at the higher energies $S \ll 1\%$. It is seen that the small extrema in S correspond to the diffraction minima of the transverse electric contribution to the cross section (cf. fig. 4). This is also true for the 7.5 MeV state where $|S|$ does not exceed 10^{-3}. However, near 60 MeV as well as at 110 MeV S shows a resonance structure instead of a simple peak or dip.

Surprisingly, the spin asymmetry is also very small for the GDR state despite its huge surface-peaked transition charge density. The explanation lies in the spin asymmetry pertaining to the magnetic scattering alone (also shown in the figure) which is out of phase with respect to the Coulombic spin asymmetry. Thus there is a considerable mutual cancellation, which also points to a strong coherence of the excitation process.

It should be remarked that the accuracy of S, being defined as a *difference* of cross sections, is much poorer than the accuracy of the cross sections. Therefore, a multiple convergence acceleration (*e.g.* fourfold) in the DWBA code is mandatory for a reliable extraction of the spin asymmetry (resulting in an accuracy of about 5%, except for the higher collision energies when S is close to zero, or for some smaller scattering angles).

The polarization correlation R is displayed in fig. 6 (bottom part). Its modulus is in general higher than $|S|$. Moreover, the extrema of R correspond to the extrema of S, sometimes with a sign reversal. Both are related to the relative dominance of the Coulomb scattering at those energies. In the regions where magnetic scattering prevails, R is, like S, reduced to values close to zero.

Figure 7 (left part) displays the angular dependence of the spin asymmetry S. For the lowest excited state we have taken collision energies of 40 and 65 MeV where $|S|$ is still comparatively large. The backward minimum for 40 MeV, known from low-energy elastic scattering [39, 40],

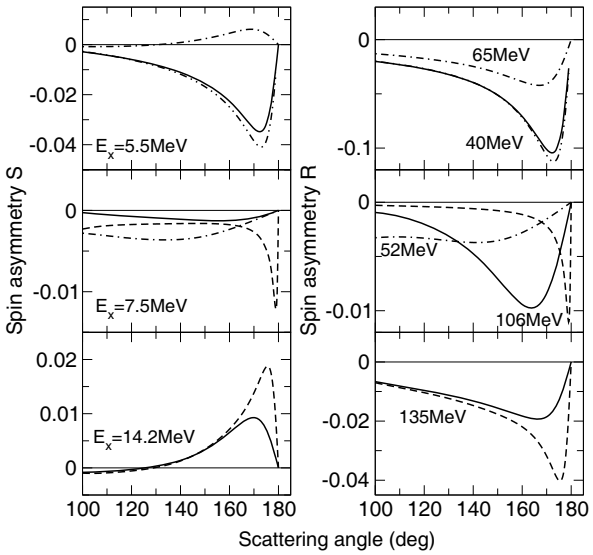

Fig. 7. Left: Sherman function S; right: polarization correlation R for the excitation of the 1^- states in ^{208}Pb as a function of scattering angle θ. Upper panels: $E_x = 5.5$ MeV at collision energies of 65 MeV (dot-dashed line) and 40 MeV (solid line). The double dot-dashed line presents the spin asymmetry for 40 MeV when recoil is neglected. Middle panels: $E_x = 7.5$ MeV at collision energies 52 MeV (dot-dashed line) and 106 MeV (solid line). Results from pure Coulomb scattering at 106 MeV are presented by the dashed line. For R, the Coulombic result has been scaled down by a factor of 0.03. Lower panels: $E_x = 14.2$ MeV at a collision energy of 135 MeV (solid line). Results from pure Coulomb scattering are given by the dashed line.

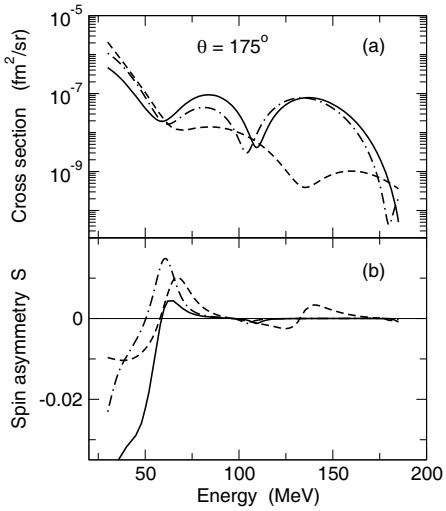

Fig. 8. (a) Differential cross section and (b) spin asymmetry for the excitation of the 1^- state at 5.5 MeV in ^{208}Pb at $\theta = 175°$ by Coulomb and transverse electric scattering. The complete results (solid line) are compared to the ones when only the magnetization $J^{\rm mag}_{1\lambda}$ (dot-dashed line) or the convection $J^{\rm conv}_{1\lambda}$ (dashed line) current density is accounted for.

has turned into a maximum in the 65 MeV predictions by the diffraction effects. The same is true for the 14.2 MeV state at impact energy 135 MeV. The spin asymmetry for the 7.5 MeV state is shown at the two collision energies 52 MeV and 106 MeV where $|S|$ has local maxima. As compared to pure Coulomb scattering, the minimum of S is shifted downward to smaller angles, the more so, the lower the collision energy. We note that for elastic scattering the extremum of S is always beyond 179° for all energies investigated.

The shift of the extremum due to the presence of the magnetic scattering holds also true for R (see fig. 7 (right part)). It should be remarked that the angular distribution of both the cross section and the spin asymmetries is less sensitive to the diffraction structures than the energy distribution. Therefore oscillations do not show up at the energies considered.

We have also studied the influence of recoil by comparing our results with those obtained by setting the mass of the nucleus to infinity. Although the recoil-based modification of the momentum k_f is negligibly small, it drastically increases Δk in eq. (7) and thus reduces the range of the radial integral, the more so, the larger E_i and the smaller θ. Again, low multipolarities are extremely sensitive to recoil effects because of the extra long range of the radial integrals. While *e.g.* for the multipolarity $L = 3$ recoil affects both cross section and spin asymmetries by less than 1% (as investigated for the lowest 3^- state at $\theta = 175°$ and energies 30–100 MeV), for $L = 1$ recoil is non-negligible at all angles and energies below 90 MeV. In particular for the 5.5 MeV state at $\theta = 175°$ and energies up to 70 MeV, the excitation cross section is changed by about 5% or less, but the recoil effect on the spin asymmetry is strong, as shown for 40 MeV in fig. 7. Beyond 100 MeV Δk is large enough to make the radial range sufficiently small so that recoil effects become unimportant.

In order to study the influence of the transition current densities on the cross section and the spin asymmetry in more detail we have performed calculations in which the current densities $J_{1\lambda}$ ($\lambda = 0, 2$) are presented by only magnetization ($J^{\rm mag}_{1\lambda}$) or only convection ($J^{\rm conv}_{1\lambda}$) components. The results are shown in fig. 8 by dot-dashed and dashed lines, respectively, for comparison with complete results (solid line). Since the magnitude of $J^{\rm mag}_{1\lambda}$ is similar to the one of $J_{1\lambda}$, there is only a slight shift of the diffraction structures in the resulting cross section as shown in fig. 8(a) for the 5.5 MeV state. However, the substitution of $J_{1\lambda}$ by $J^{\rm mag}_{1\lambda}$ has a large effect on the spin asymmetry, even changing its sign at the backmost angles between 50 MeV and 60 MeV. The convection current densities are about an order of magnitude weaker than $J^{\rm mag}_{1\lambda}$ for this state such that, if only they are retained, the relative importance of the charge density ϱ_1 increases. This leads to a strongly reduced cross section above 70 MeV (except in the diffraction minima, see fig. 8(a)), but to a much larger spin asymmetry (see fig. 8(b)).

5 Conclusion

We have given predictions for the differential cross sections and for the transverse spin asymmetries S and R of

dipole excitations of ^{208}Pb by the impact of electrons polarized perpendicular to the beam axis. This was achieved by calculating the nuclear transition densities within the quasiparticle phonon model and by applying the DWBA scattering formalism.

For the lowest dipole state investigated, with its large transition current densities, we have found that for scattering angles above 170° and collision energies beyond 70 MeV the cross section is strongly dominated by the magnetic scattering amplitude. This leads to a considerable quenching of the transverse spin asymmetries to values well below 1%.

For the PDR state at 7.5 MeV, for which the transition charge density even falls below the transition current densities near the nuclear surface, the moduli of S and R are smaller than 4×10^{-3} and 10^{-2}, respectively, at all angles and energies considered.

The highest excited state considered is the only one which, due to its dominating transition charge density and constructively interfering collectivity, shows an appreciable spin asymmetry beyond 100 MeV collision energy. In fact, the maxima of $|S| \sim 0.01$ and $|R| \sim 0.02$ occur near 135 MeV.

Besides the quenching, the presence of magnetic scattering also leads to a considerable shift of the backward scattering angle which pertains to the largest spin asymmetry. No longer is the extremum of S beyond 179° as for elastic scattering but is, for example, reduced to 170° for the GDR state excited by 135 MeV electrons, or even shifted down to 130° for the PDR state at 52 MeV impact energy.

In a proof-of-principle measurement both $|S|$ and the cross section should be large. We therefore suggest an investigation of the 5.5 MeV state near 40 MeV at a scattering angle of about 172° (with $S \approx -0.035$ and $\mathrm{d}\sigma/\mathrm{d}\Omega \approx 2.5 \times 10^{-7}\,\mathrm{fm}^2/\mathrm{sr}$). The effect of the diffraction structures, the change of the minimum of S into a maximum, is only accessible at collision energies beyond 60 MeV. This might be achieved by choosing an energy of 65 MeV for this state ($S = 6.1 \times 10^{-3}$ at 169°) or to measure the GDR state at 135 MeV ($S = 9.3 \times 10^{-3}$ at 170°). However, this is at the expense of smaller cross sections ($4.4 \times 10^{-8}\,\mathrm{fm}^2/\mathrm{sr}$ for the 5.5 MeV state and $6.5 \times 10^{-9}\,\mathrm{fm}^2/\mathrm{sr}$ for the 14.2 MeV state).

By evaluating the scattering theory separately for the magnetization contribution and for the convection contribution to the transition current densities we were able to study the effect of changes in $J_{1\lambda}$ on both differential cross section and spin asymmetry. As a result we have confirmed that S is indeed far more sensitive to such changes than the cross section. Its measurement therefore offers the possibility for a refined test of the nuclear models.

DHJ would like to thank Prof. J. Enders for initiating this work and for encouraging discussions. VYuP acknowledges support by the DFG (Contracts No. SFB 1245) and stimulative discussions with Prof. J. Wambach.

Appendix A.

We derive the asymptotic splitting of the radial Dirac functions into a sum of two terms, one behaving like e^{ikz}, the other like e^{-ikz} (with k equal to k_i or k_f).

Using the representation of g_κ and f_κ in terms of regular (F_γ) and irregular (G_γ) non-relativistic Coulomb waves [31] (where $\gamma = \sqrt{\kappa^2 - (Z_T/c)^2}$ and $Z_T > 0$ is the nuclear charge number) one has

$$\begin{aligned}\begin{pmatrix} g_\kappa^{\mathrm{reg}}(r) \\ g_\kappa^{\mathrm{irr}}(r) \end{pmatrix} &= \frac{N_\kappa}{kr}\left[(\kappa+\gamma)\sqrt{\gamma^2+\eta^2}\,kc \begin{pmatrix} F_\gamma(\eta,kr) \\ G_\gamma(\eta,kr)\end{pmatrix}\right. \\ &\quad \left. - \frac{Z_T}{c}\,(\gamma c^2 - \kappa E) \begin{pmatrix} F_{\gamma-1}(\eta,kr) \\ G_{\gamma-1}(\eta,kr)\end{pmatrix}\right], \\ N_\kappa &= \sqrt{\frac{E+c^2}{\pi E}}\,\mathrm{sign}\;\kappa\,\frac{1}{\gamma} \\ &\quad \times \frac{1}{\sqrt{(Z_T/c)^2(E+c^2)^2 + (\kappa+\gamma)^2(kc)^2}}\,, \end{aligned} \tag{A.1}$$

where $E = \sqrt{k^2c^2 + c^4}$ (with k equal to k_i or k_f) is the total energy and $\eta = Z_T E/(kc^2)$ is the Sommerfeld parameter. A similar expression holds for the small components,

$$\begin{aligned}\begin{pmatrix} f_\kappa^{\mathrm{reg}}(r) \\ f_\kappa^{\mathrm{irr}}(r) \end{pmatrix} &= -\frac{N_\kappa}{kr}\left[-\frac{Z_T}{c}\,\sqrt{\gamma^2+\eta^2}\,kc \begin{pmatrix} F_\gamma(\eta,kr) \\ G_\gamma(\eta,kr)\end{pmatrix}\right. \\ &\quad \left. + (\kappa+\gamma)(\gamma c^2 - \kappa E) \begin{pmatrix} F_{\gamma-1}(\eta,kr) \\ G_{\gamma-1}(\eta,kr)\end{pmatrix}\right]. \end{aligned} \tag{A.2}$$

We note that the normalization in (A.1) and (A.2) has been chosen such that $g_\kappa^{\mathrm{reg}} \equiv \sqrt{\frac{E+c^2}{\pi E}}\,\frac{1}{kr} \cdot G_\kappa^{\mathrm{reg}}$ [32], where G_κ^{reg} stands for the large component of the regular Coulomb-Dirac function being asymptotically plane-wave normalized (with unit amplitude) as done in the Salvat code [31].

For large distances the asymptotic expansions of F_γ ($= g\cos\theta_\gamma + f\sin\theta_\gamma$) and G_γ ($= f\cos\theta_\gamma - g\sin\theta_\gamma$) [41] may be used, which readily can be continued into the complex plane. Then, from (5) for $|z|$ large,

$$\begin{aligned} g_\kappa(z) = \frac{N_\kappa}{kz}\left\{-ie^{i\delta_\kappa}\frac{1}{2}\,[c_1 C_\gamma(z) - c_2 C_{\gamma-1}(z)]\right. \\ \left. + ie^{-i\delta_\kappa}\frac{1}{2}\left[c_1 C_\gamma^{\mathrm{conj}}(z) - c_2 C_{\gamma-1}^{\mathrm{conj}}(z)\right]\right\}, \end{aligned} \tag{A.3}$$

where $c_1 = (\kappa+\gamma)\sqrt{\gamma^2+\eta^2}\,kc$ and $c_2 = \frac{Z_T}{c}\,(\gamma c^2 - \kappa E)$.

The functions C_γ and $C_\gamma^{\rm conj}$ are defined by

$$C_\gamma(z) = e^{i\theta_\gamma(z)}\,(f+ig)(z)$$
$$C_\gamma^{\rm conj}(z) = e^{-i\theta_\gamma(z)}\,(f+ig)^*(z), \qquad (A.4)$$

where

$$\theta_\gamma(z) = kz+\eta\ln 2kz-\gamma\pi/2+\ \arg\,\Gamma(\gamma+1-i\eta) \qquad (A.5)$$

and [41]

$$(f+ig)(z) = 1+\frac{(-i\eta-\gamma)(-i\eta+\gamma+1)}{2ikz}+\dots$$
$$(f+ig)^*(z) = 1+\frac{(i\eta-\gamma)(i\eta+\gamma+1)}{-2ikz}+\dots, \qquad (A.6)$$

which is rapidly converging for γ not too large (otherwise R_m has to be increased). Likewise, the small component is written as

$$f_\kappa(z) = -\frac{N_\kappa}{kz}\,\Big\{-ie^{i\delta_\kappa}\,\frac{1}{2}\,[d_1C_\gamma(z)+d_2C_{\gamma-1}(z)]$$
$$+\,ie^{-i\delta_\kappa}\,\frac{1}{2}\,\Big[d_1C_\gamma^{\rm conj}(z)+d_2C_{\gamma-1}^{\rm conj}(z)\Big]\Big\}, \qquad (A.7)$$

with $d_1 = -\frac{Z_T}{c}\sqrt{\gamma^2+\eta^2}\,kc$ and $d_2 = (\kappa+\gamma)(\gamma c^2-\kappa E)$.

Since $e^{i\theta_\gamma(z)}\sim e^{ikz}$, the function $g_\kappa^{(+)}(e^{ikz})$ as defined in (6) comprises the first line of (A.3), and $g_\kappa^{(-)}(e^{-ikz})$ is given by the second line of (A.3). Similarly the two lines in (A.7) define $f_\kappa^{(+)}(e^{ikz})$, respectively $f_\kappa^{(-)}(e^{-ikz})$.

References

1. R.M. Laszewski, P. Axel, Phys. Rev. C **19**, 342 (1979).
2. R.M. Laszewski, Phys. Rev. C **34**, 1114 (1986).
3. R.-D. Herzberg, P. von Brentano, J. Eberth, J. Enders, R. Fischer, N. Huxel, T. Klemme, P. von Neumann-Cosel, N. Nicolay, N. Pietralla, V.Yu. Ponomarev, J. Reif, A. Richter, C. Schlegel, R. Schwengner, S. Skoda, H.G. Thomas, I. Wiedenhover, G. Winter, A. Zilges, Phys. Lett. B **390**, 49 (1997).
4. K. Govaert, F. Bauwens, J. Bryssinck, D. De Frenne, E. Jacobs, W. Mondelaers, L. Govor, V.Yu. Ponomarev, Phys. Rev. C **57**, 2229 (1998).
5. D. Savran, M. Babilon, A.M. van den Berg, M.N. Harakeh, J. Hasper, A. Matic, H.J. Wörtche, A. Zilges, Phys. Rev. Lett. **97**, 172502 (2006).
6. J. Endres, E. Litvinova, D. Savran, P.A. Butler, M.N. Harakeh, S. Harissopulos, R.-D. Herzberg, R. Krucken, A. Lagoyannis, N. Pietralla, V.Yu. Ponomarev, L. Popescu, P. Ring, M. Scheck, K. Sonnabend, V.I. Stoica, H.J. Wörtche, A. Zilges, Phys. Rev. Lett. **105**, 212503 (2010).
7. P. Adrich, A. Klimkiewicz, M. Fallot, K. Boretzky, T. Aumann, D. Cortina-Gil, U. Datta Pramanik, Th.W. Elze, H. Emling, H. Geissel, M. Hellström, K.L. Jones, J.V. Kratz, R. Kulessa, Y. Leifels, C. Nociforo, R. Palit, H. Simon, G. Surówka, K. Sümmerer, W. Waluś, Phys. Rev. Lett. **95**, 132501 (2005).
8. F.C.L. Crespi *et al.*, Phys. Rev. Lett. **113**, 012501 (2014).
9. D. Savran, T. Aumann, A. Zilges, Prog. Part. Nucl. Phys. **70**, 210 (2013).
10. H. Gräf, V. Heil, A. Richter, E. Spamer, W. Stock, O. Titze, Phys. Lett. B **72**, 179 (1977).
11. D. Meuer, R. Frey, D.H.H. Hoffmann, A. Richter, E. Spamer, O. Titze, W. Knüpfer, Nucl. Phys. A **349**, 309 (1980).
12. C. Lüttge, C. Hofmann, J. Horn, F. Neumeyer, A. Richter, G. Schrieder, E. Spamer, A. Stiller, D.I. Sober, S.K. Matthews, L.W. Fagg, Nucl. Instrum. Methods A **366**, 325 (1995).
13. Y. Poltoratska, R. Barday, U. Bonnes, M. Brunken, C. Eckardt, R. Eichhorn, J. Enders, C. Heßler, C. Ingenhaag, W.F.O. Müller, M. Platz, M. Roth, B. Steiner, M. Wagner, T. Weiland, AIP Conf. Proc. **1149**, 715 (2009).
14. S.T. Tuan, L.E. Wright, D.S. Onley, Nucl. Instrum. Methods **60**, 70 (1968).
15. N. Ryezayeva, T. Hartmann, Y. Kalmykov, H. Lenske, P. von Neumann-Cosel, V.Yu. Ponomarev, A. Richter, A. Shevchenko, S. Volz, J. Wambach, Phys. Rev. Lett. **89**, 272502 (2002).
16. J. Enders, P. von Brentano, J. Eberth, A. Fitzler, C. Fransen, R.-D. Herzberg, H. Kaiser, L. Kaubler, P. von Neumann-Cosel, N. Pietralla, V.Yu. Ponomarev, A. Richter, R. Schwengner, I. Wiedenhover, Nucl. Phys. A **724**, 243 (2003).
17. J. Sromicki, K. Bodek, D. Conti, St. Kistryn, J. Lang, S. Navert, O. Naviliat-Cuncic, E. Stephan, C. Sys, J. Zejma, W. Haeberli, E. Reichert, M. Steigerwald, Phys. Rev. Lett. **82**, 57 (1999).
18. S. Abrahamyan *et al.*, Phys. Rev. Lett. **109**, 192501 (2012).
19. H. Überall, *Electron Scattering from Complex Nuclei* (Academic Press, New York, 1971).
20. E. Moya de Guerra, Phys. Rep. **138**, 293 (1986).
21. T.W. Donnelly, A.S. Raskin, Ann. Phys. **169**, 247 (1986).
22. C.M. Vincent, H.T. Fortune, Phys. Rev. C **2**, 782 (1970).
23. V.A. Yerokhin, A. Surzhykov, Phys. Rev. A **82**, 062702 (2010).
24. F. Gross, *Relativistic Quantum Mechanics and Field Theory* (Wiley, New York, 1993) p. 286.
25. K. Alder, A. Bohr, T. Huus, B. Mottelson, A. Winther, Rev. Mod. Phys. **28**, 432 (1956).
26. R.S. Willey, Nucl. Phys. **40**, 529 (1963).
27. H.C. Lee, Atomic Energy of Canada, Rep. AECL-4839, Ontario (1975).
28. J. Heisenberg, H.P. Blok, Annu. Rev. Nucl. Part. Sci. **33**, 569 (1983).
29. A.R. Edmonds, *Angular Momentum in Quantum Mechanics*, 2nd edition (Princeton University Press, Princeton, 1960) sect. 5.9.
30. H.De Vries, C.W.De Jager, C.De Vries, At. Data Nucl. Data Tables **36**, 495 (1987).
31. F. Salvat, J.M. Fernández-Varea, W. Williamson Jr., Comput. Phys. Commun. **90**, 151 (1995).
32. D.H. Jakubassa-Amundsen, Nucl. Phys. A **937**, 65 (2015).
33. D.R. Yennie, D.G. Ravenhall, R.N. Wilson, Phys. Rev. **95**, 500 (1954).
34. H.T. Fortune, T.J. Gray, W. Trost, N.R. Fletcher, Phys. Rev. **179**, 1033 (1969).
35. V.G. Soloviev, *Theory of Atomic Nuclei: Quasiparticles and Phonons* (Institute of Physics, Bristol, 1992).

36. D.H. Jakubassa-Amundsen, R. Barday, J. Phys. G **39**, 025102 (2012).
37. P. Sarriguren, E. Moya de Guerra, Phys. Rev. C **30**, 2105 (1984).
38. M. Nishimura, E. Moya de Guerra, D.W.L. Sprung, Nucl. Phys. A **435**, 523 (1985).
39. J.W. Motz, H. Olsen, H.W. Koch, Rev. Mod. Phys. **36**, 881 (1964).
40. P. Uginčius, H. Überall, G.H. Rawitscher, Nucl. Phys. A **158**, 418 (1970).
41. M. Abramowitz, I.A. Stegun, *Handbook of Mathematical Functions* (Dover Publications, New York, 1964) sect. 14.